

# Symmetry of the $1s$ core exciton in diamond studied using x-ray Raman scattering

S. Galambosi,<sup>1</sup> J. A. Soininen,<sup>1</sup> K. Nygård,<sup>1</sup> S. Huotari,<sup>2</sup> and K. Hämäläinen<sup>1</sup>

<sup>1</sup>*Division of X-ray Physics, Department of Physical Sciences, University of Helsinki, P.O. Box 64, FIN-00014 University of Helsinki, Finland*

<sup>2</sup>*European Synchrotron Radiation Facility, Boîte Postale 220, F-38043 Grenoble, France*

(Received 23 March 2007; revised manuscript received 16 August 2007; published 14 November 2007)

The detailed electronic structure of diamond has been studied by x-ray Raman scattering at the  $1s$  excitation threshold. By combining the experimental high-resolution inelastic scattering spectra with a computational scheme based on the real-space multiple scattering approach, the symmetry-resolved  $s$  and  $p$  angular projected unoccupied local densities of states of diamond have been extracted. The results unambiguously show that the extensively studied diamond  $1s$  core exciton has a  $p$ -like angular symmetry. Furthermore, the effects of various experimental and numerical uncertainties on the extraction scheme are carefully analyzed and discussed giving important insight to the applicability of this promising complementary technique to other systems.

DOI: [10.1103/PhysRevB.76.195112](https://doi.org/10.1103/PhysRevB.76.195112)

PACS number(s): 78.70.Ck, 71.35.-y, 71.20.Mq

## I. INTRODUCTION

Diamond is a wide gap semiconductor having a relatively simple crystal and electronic structure. Although mainly known for its hardness, doped diamond has also been shown to exhibit other fascinating physical properties. Using boron dopants, for example, diamond becomes superconductive,<sup>1</sup> while the nitrogen-vacancy center in diamond is a promising candidate for solid state quantum communication applications.<sup>2-4</sup> To comprehend how the physical characteristics are affected by dopants, it is extremely important to deeply understand the detailed electronic structure of pure diamond. Most optical and electric properties of diamond are well described by theoretical computations.<sup>5-9</sup> From the experimental point of view, x-ray absorption spectroscopy (XAS) is a well known technique for probing the electronic structure. The experimental XAS spectra of diamond are, for most parts, well reproduced by theoretical computations that incorporate a proper treatment of the electron-hole interactions.<sup>10-12</sup> However, even these state of the art calculations heavily overestimate the spectral weight over a range of a few eV's above the carbon  $1s$  excitation threshold. The cause of this overestimation is currently unknown.

The carbon  $K$  edge in diamond has attracted considerable interest since the discovery of the  $1s$  core exciton.<sup>13</sup> The interest has been partly fueled by the apparent similarity between a nitrogen impurity and the carbon atom having an effective charge of  $Z+1$  due to the presence of the core hole. Surprisingly, the published results concerning the nature of the exciton have been somewhat controversial. The experimental exciton binding energy of 0.19 eV was well reproduced by hydrogenic effective-mass theory.<sup>13,14</sup> This interpretation was, however, questioned by Jackson and Pederson<sup>15</sup> who predicted a deep  $s$ -like ground state for the exciton. The excitation of the  $1s$  electron into this state is dipole forbidden. Consequently, the electron gets excited into a shallow  $p$ -like state. Based on experimental results, Nithianandam argued<sup>16</sup> that the observed exciton is  $s$ -like and that the observation of this nondipole excitation is made possible by the intervalley mixing of states. The first direct evidence on the symmetry of the exciton was obtained by

Batson.<sup>17</sup> Using symmetry-selected electron-energy-loss spectroscopy, no evidence was found for an even parity excitonic state. Moreover, the experimental result was found to support the delocalized exciton picture.

With the availability of intense synchrotron radiation sources, x-ray Raman scattering<sup>18</sup> (XRS) has become a significant complementary technique to x-ray absorption spectroscopy. XRS is a versatile technique that can be used to study the electronic structure of a variety of materials such as solids,<sup>19</sup> organic materials,<sup>20</sup> and liquids.<sup>21</sup> However, in contrast to XAS, the utilization of the XRS method enables the relative contributions of dipole versus non-dipole transitions in the spectra to be tuned by varying the momentum transfer during the scattering process. Valuable information on the electronic states of the system can be obtained by comparing the evolution of the experimental and theoretically calculated XRS spectra as a function of the momentum transfer.<sup>22-24</sup> Additional information can be extracted from the momentum transfer dependence of the XRS spectra by the scheme proposed by Soininen *et al.*<sup>25</sup> The authors pointed out that the transition matrix elements of a core electron excitation can be computed with a good accuracy. These matrix elements can then be combined with the experimental spectra to extract the angular momentum projected local density of states ( $\ell$ -DOS) in the core-excited system. This scheme has recently been applied to various hard<sup>26,27</sup> and soft condensed matter<sup>20</sup> systems.

The current method for analyzing the angular symmetry of the core exciton has several benefits. First, experimentally it is very simple to control the relative weights of nondipole transitions in the spectra by changing the scattering angle of the photons. Second, the interpretation of the final-state symmetry is straightforward. In the method of Batson,<sup>17</sup> only the final-state parity could be chosen. In the current method, the exact angular symmetry of the final state is selected. Finally, the only theoretical input needed for the analysis of the experimental data are the transition matrix elements. Thus, the theoretical computation of the full XRS spectra is not necessary.

In this paper, we report measurements of the momentum transfer dependent XRS spectra of diamond near the carbon

1s excitation threshold. We have applied the aforementioned scheme to extract the *s*- and *p*-type  $\ell$ -DOS from the experimental data. The structure of this paper is as follows. First, we briefly review the theoretical background of XRS and the angular momentum projected decomposition scheme. Next, we describe the experimental details. We then discuss our results and their implications on the interpretation of the core exciton. Finally, we address the reliability of the decomposition scheme with respect to some experimental factors.

## II. THEORETICAL BACKGROUND

In nonresonant XRS experiments, hard x rays are scattered by the sample. The energy of the incident rays is typically in the order of 10 keV and is far from any absorption edge of the target system. In the scattering process, the energy transferred ( $\omega$ ) to the sample is close to a core electron binding energy. The photon also transfers momentum ( $\mathbf{q}$ ) to the system. The scattering cross section of XRS is proportional to the dynamic structure factor  $S(\mathbf{q}, \omega)$ ,<sup>18</sup> which, using the quasiparticle approximation together with the Fermi golden rule, can be expressed as

$$S(\mathbf{q}, \omega) = \sum_f |\langle f | e^{i\mathbf{q}\cdot\mathbf{r}} | i \rangle|^2 \delta(\omega + E_i - E_f), \quad (1)$$

where  $E_i$  and  $E_f$  correspond to the quasiparticle energies of the electron in the initial  $|i\rangle$  and final  $|f\rangle$  state. In the small  $q$  limit, the exponential in Eq. (1) can be approximated by expanding it up to linear order in  $\mathbf{q}$ . As shown by Mizuno and Ohmura,<sup>28</sup> the spectral shape of XRS in this limit is governed by the same dipole-allowed transition matrix elements as in x-ray absorption spectroscopy. Thus XRS measured at low  $q$  can be used as an alternative to XAS.<sup>29,30</sup> As  $q$  is increased, higher order terms giving rise to nondipole transitions have to be retained in the expansion. This possibility to control the relative contributions of dipole versus nondipole-allowed transitions in the spectrum makes XRS a versatile and unique tool to study the electronic structure of matter.

Due to the random orientation of the crystallites in a polycrystalline substance, an angular average of the dynamic structure factor is measured when using powder samples. In this case,  $S(\mathbf{q}, \omega)$  can be reformulated into a particularly simple form using the real-space multiple scattering formalism,<sup>25,26</sup>

$$S(\mathbf{q}, \omega) = \sum_l |M_l(q, E)|^2 \rho_l(E). \quad (2)$$

Here,  $M_l(q, E)$  is the matrix element for a transition from the initial core state into an excited state,  $\rho_l(E)$  the local density of the unoccupied core-excited states, and  $E = \omega + E_i$  the final-state energy. The angular momentum channels are denoted by  $l=0, 1, 2, \dots$ . This equation is the starting point for our analysis of the experimental spectra. According to Eq. (2), the dynamic structure factor is essentially a linear combination of the angular momentum projected local densities of states of the excited state ( $\ell$ -DOS)  $\rho_l(E)$  weighted by the square of the corresponding transition matrix elements  $M_l$ .

The set of linear equations in Eq. (2) may be solved to find  $\rho_l$ . Equation (2) can be recast into a matrix form  $\mathbf{S} = \mathbf{M}\rho$ , which holds for each energy point in the spectra,

$$\begin{pmatrix} S(q_1) \\ S(q_2) \\ \vdots \end{pmatrix} = \begin{pmatrix} |M_0(q_1)|^2 & |M_1(q_1)|^2 & \dots \\ |M_0(q_2)|^2 & |M_1(q_2)|^2 & \dots \\ \vdots & \vdots & \ddots \end{pmatrix} \begin{pmatrix} \rho_0 \\ \rho_1 \\ \vdots \end{pmatrix}. \quad (3)$$

When experimental spectra are available at more  $q$  values than the number of angular momentum  $l$  elements in  $\rho$ , the overdetermined equation may be solved in the least-squares sense. The effect of finite statistical accuracy and other experimental uncertainties on the inversion will be addressed later in this paper. For this work, the transition matrix elements needed for the inversion of Eq. (2) were calculated using an extension<sup>25</sup> of the FEFF8.2 program.<sup>31,32</sup>

## III. EXPERIMENT

The experiments were performed on beamline ID16 at the European Synchrotron Radiation Facility (Grenoble, France). The x-ray Raman scattering spectra were obtained by scanning the incident energy with respect to the analyzed energy (12.4 keV) selected via the use of the (880) reflection of a spherically bent Ge(110) crystal on the Rowland circle (diameter of 1 m) in a near backscattering geometry. The analyzed energy was chosen such that large enough momentum transfer values could be accessed. Using the Ge analyzer, a total energy resolution of 0.60 eV was determined from the full width at half maximum of the quasielastic line. The momentum resolution varied from  $\Delta q = 0.4$  a.u. at  $q = 0.6$  a.u. to 0.1 a.u. at 6.3 a.u., as determined by the finite size of the analyzer crystal. An energy region spanning about 10 eV around the core exciton was measured with an improved energy resolution of 0.3 eV. The resolution enhancement was achieved by limiting the angular acceptance of the analyzer crystal.

Synthetic diamond powder (99.9%, Alfa Aesar) with a grain size  $< 1 \mu\text{m}$  was used in the experiments. The powder was gently pressed into a cylindrical pellet shape in a sample holder. All measurements were carried out at room temperature.

The momentum transfers were selected such that the carbon *K*-edge x-ray Raman spectra were well separated from the maximum of the Compton profile. The remaining background was subtracted by calculating the diamond Compton profile using a modification of the STOBED-MON (Ref. 33) package and fitting it to the experimental spectra. This approach to the background subtraction was previously used and found to work well in Ref. 20. The experimental spectra were also corrected for absorption, detector dead time, and energy dependence of the incident flux, although these factors contribute only a few percent over the measured energy range.

## IV. RESULTS AND DISCUSSION

The x-ray Raman scattering spectra at the carbon *K* edge of diamond was measured using three distinct values of  $q$ .

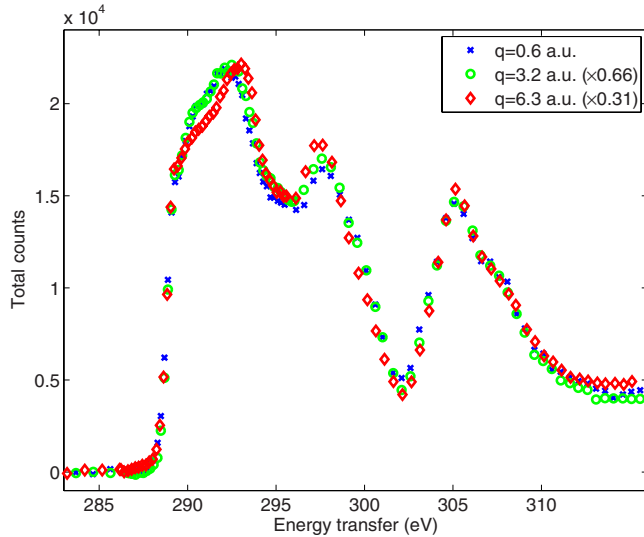


FIG. 1. (Color online) The experimental x-ray Raman scattering spectra near the carbon  $K$  edge in diamond using three different  $q$  values. The shown spectra are normalized to the same area.

The background subtracted spectra normalized to the same area are shown in Fig. 1. The small momentum transfer spectrum contains mainly dipole-allowed transitions. Consequently, it corresponds well with the reported x-ray absorption spectra.<sup>13,34–36</sup> The large dip around 301 eV is associated with the second band gap of diamond.<sup>5</sup> With the current energy resolution, the core exciton is barely visible as a small shoulder near 289 eV. The slight changes in the spectra at higher  $q$  values reflect the changes in the weighting of various transition channels contributing to the spectra.

Using our FEFF calculations, we have estimated the relative spectral contribution of transitions into  $s$ -,  $p$ -, and  $d$ -like final states. The contributions of various transition channels are shown in Table I for three momentum transfer values. These figures were obtained by integrating each angular momentum projected component of the theoretically computed atomic spectra between 280 and 315 eV. Clearly, even at the moderate momentum transfer of 3.2 a.u., the XRS spectra are heavily dominated by dipole-allowed transitions. This is also visible in Fig. 1 where the spectra measured at  $q=0.6$  and 3.2 a.u. are essentially identical. This confirms that XRS can indeed be used as an alternative to soft x-ray absorption spectroscopy even at moderate  $q$  values. This is highly beneficial as the intensity of XRS scales quadratically with  $q$ , and thus larger momentum transfer values result in enhanced count rates.

TABLE I. The relative intensity of different transition channels in the XRS spectra at three momentum transfer values estimated from the FEFF calculations.

$q$ (a.u.)	$s \rightarrow s$	$s \rightarrow p$	$s \rightarrow d$
0.6	0.004	0.995	0.001
3.2	0.11	0.88	0.01
6.3	0.35	0.64	0.01

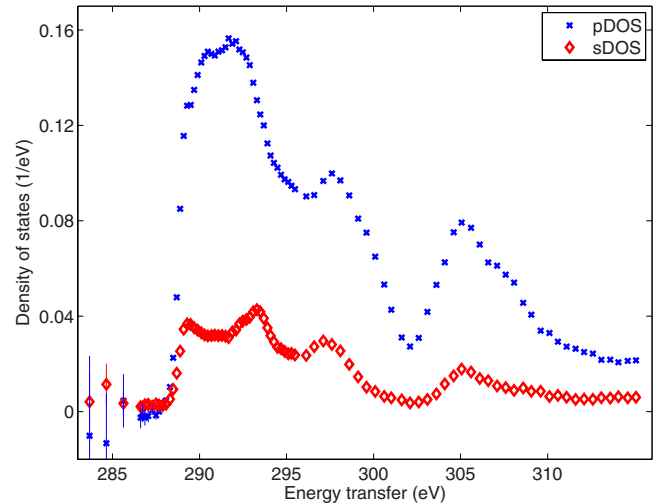


FIG. 2. (Color online) The angular momentum projected density of states as obtained from the experimental data. The error bars reflect the effect of the finite statistical accuracy of the experimental data. The error bars are shown for data points where the uncertainty exceeds the size of the marker.

Prior to applying Eq. (3) in order to extract the  $\ell$ -DOS, the dynamic structure factors derived from the experimental spectra have to be properly normalized. This could be easily accomplished by applying the so-called  $f$ -sum rule<sup>37</sup> utilizing the total integrated area for the normalization. However, in practice, this is somewhat problematic as the x-ray Raman spectra are typically recorded only over a restricted energy range. In the following, we have chosen to normalize the spectra with respect to the theoretically calculated atomic background  $S_0(\mathbf{q}, \omega)$ .<sup>25,38</sup> This quantity is the dynamic structure factor for an atom embedded in the target system with the intensity modulation due to the neighboring scatterers neglected. The experimental and theoretical spectra at each  $q$  value were normalized to the same area over a finite energy window,

$$\int_{E_{min}}^{E_{max}} S_{exp}(\mathbf{q}, \omega) = \int_{E_{min}}^{E_{max}} S_0(\mathbf{q}, \omega). \quad (4)$$

The effect of integration window and other ways to normalize the spectra will be addressed later in this paper.

In this work, we considered only the  $s$ - and  $p$ -type final states of carbon. Our FEFF calculations indicate that the density of  $d$  states is of similar magnitude as the  $s$ -DOS. However, as visible from Table I, the transitions into  $d$ -type final states have only a minor contribution to the XRS spectra due to the small transition matrix elements. The inclusion of  $d$ -type states in the matrix inversion resulted in essentially unchanged  $s$ - and  $p$ -DOS together with an unphysically large density of  $d$  states. The  $s$ - and  $p$ -DOS shown in Fig. 2 were solved by using the three experimental spectra shown in Fig. 1 and inverting the overdetermined Eq. (3) in the least-squares sense. The very close resemblance of the  $p$ -DOS to the shape of the experimental spectra again reflects the major contribution of dipole-allowed transitions. The intensity en-

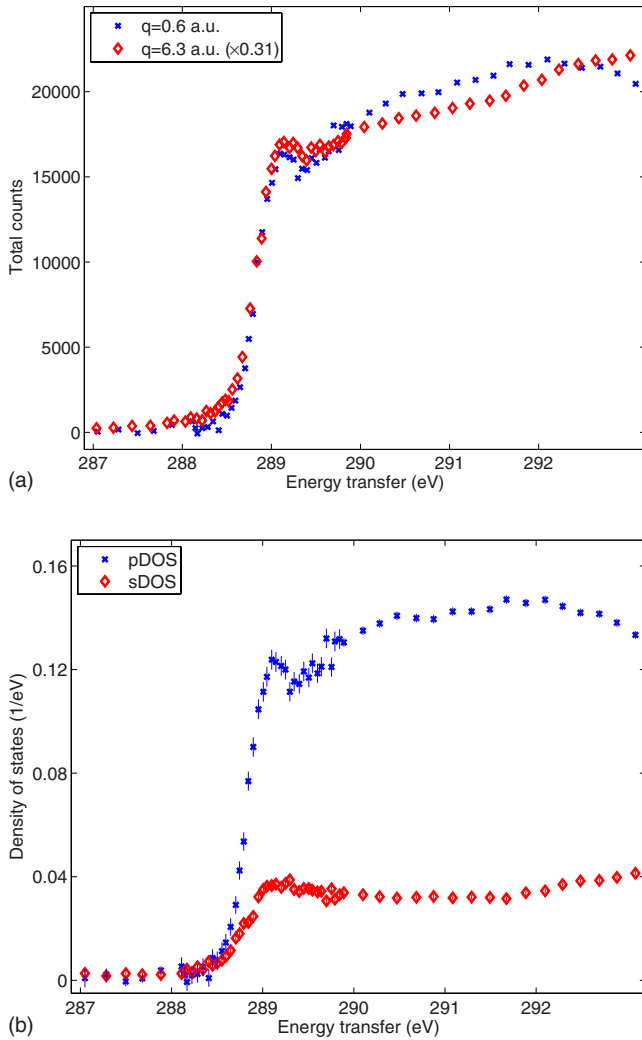


FIG. 3. (Color online) (a) The momentum transfer dependence of the experimental XRS spectra measured with a 0.3 eV energy resolution and (b) the experimental  $\ell$ -DOS in the near edge region.

hancement of the XRS spectra near 293 eV at larger  $q$  values can be explained by the peak in the  $s$ -DOS in that energy region.

To evaluate the  $q$  dependence of the  $1s$  core exciton, the near edge regime was measured with an improved energy resolution of 0.3 eV using two values of  $q$ . The momentum transfer dependence of the resulting XRS spectra is shown in Fig. 3(a). The high-resolution part of the spectra is visible as a region of increased statistical noise due to the lower total number of photons collected. The spectra in the figure can be regarded as the sum of two components, the excitonic transition which is superimposed on the contribution of transitions into continuum states.<sup>13,39</sup> Figure 3(a) seems to imply that the momentum transfer dependence of the spectra mainly originates from the changes in the broad continuum part of the spectra. This is confirmed by Fig. 3(b) which shows the  $\ell$ -DOS of the same energy region. Clearly, the sharp excitonic feature shows up only in the  $p$ -DOS demonstrating unambiguously that the exciton has a  $p$ -like symmetry. This is in a clear contrast with the  $s$ -type exciton sug-

gested by the experimental work of Nithianandam.<sup>16</sup> According to the calculations of Jackson and Pederson,<sup>15</sup> the observed  $p$ -like state could be explained as being an excited state of the  $s$ -like ground state of the exciton. This implies that at larger momentum transfer values, we should observe an additional, lower lying feature. This should also show up as a peak in the  $s$ -DOS. However, as pointed out by Mauri and Car,<sup>40</sup> the theoretical energy difference between the  $s$ -like ground state and the  $p$ -like excited state of the exciton is only 0.13 eV in the ideal, nondistorted diamond lattice. With the current experimental energy resolution of about 0.3 eV, we do not observe evidence for the  $s$ -like excitonic state. In this respect, our experimental results are in line with the earlier findings of Batson.<sup>17</sup>

In order to address the reliability of this technique, we have carried out several tests to estimate how various experimental and numerical factors affect the accuracy of the  $\ell$ -DOS extraction process. In this paper, we will consider the following factors: the finite counting statistics of the experimental data, the background subtraction and normalization of the data, the convergence of the computations, and shifts in the energy scales between the experimental and calculated spectra.

The dynamic structure factors in Eq. (3) are derived from the experimental data. Thus,  $S(q)$  contains statistical noise which, consequently, is reflected as a finite statistical accuracy in the extracted density of states  $\rho$ . Using standard error propagation formulas,<sup>41</sup> the variance of the fluctuations in  $\rho$  can be calculated from

$$\sigma^2(\rho_i) = (\mathbf{m}^T \mathbf{m})_{ii}^{-1}, \quad (5)$$

where  $\mathbf{m}$  is the scaled transition matrix having elements  $m_{ij} = |M_j(q_i)|^2 / \sigma_i$ , with  $\sigma_i$  representing the standard deviation of the statistical fluctuations in  $S(q_i)$ . The inversion in Eq. (5) refers to the pseudoinverse<sup>42</sup> of  $\mathbf{m}^T \mathbf{m}$  in case of the overdetermined Eq. (3). The error bars in Figs. 2 and 3(b) were estimated using Eq. (5). The increasing size of the error bars at low energies is due to the diminishing value of the transition matrix elements, which tends to amplify the statistical fluctuation in the data. We also performed numerical simulations by generating statistical errors to the experimental data and performing the inversion. The standard deviation of the extracted  $\ell$ -DOS calculated from  $10^3$  of this kind of simulated spectra was consistent with the one obtained from the analytical calculation.

In order to obtain  $S(\mathbf{q}, \omega)$  corresponding to the  $1s$  electron excitation, the contribution of other electrons in the XRS spectra has to be subtracted. While this contribution is generally not linear, it is typically a smooth and slowly varying function of the energy transfer. The background subtracted spectra have to be normalized on an absolute scale. As previously mentioned, this is somewhat problematic due to the finite energy range measured. In addition to the atomic background  $S_0(\mathbf{q}, \omega)$ , we also performed tests normalizing against the theoretical full XRS spectra calculated using the FEFF extension or using the  $f$ -sum rule. Moreover, we varied the energy window used in the normalization. According to our results, the effect of all these factors is to slightly modify the

absolute intensity of the obtained  $\ell$ -DOS. However, we emphasize that the shape of the  $\ell$ -DOS remains essentially unchanged. This is natural, since the choice of normalization is effectively a scaling factor, whereas the incorrect subtraction of a slowly varying background can induce an additional, slight slope in the  $\ell$ -DOS.

As previously mentioned, the transition matrix elements in this work were computed using a modification of the FEFF program. Since these matrix elements are essentially atomic properties of the scatterer, they converge very rapidly as a function of the cluster size. The matrix elements remain largely unchanged when the calculations are carried out using cluster sizes exceeding 70 atoms. On the other hand, due to the slow convergence of the theoretically computed DOS, the calculated XRS spectrum is slow to converge. Our tests imply that while the changes are small, the XRS spectra calculated using 380 atoms have still not fully reached convergence. The transition matrix elements used in the analysis were computed using a cluster size of 274 atoms.

Finally, a shift between the energy scales of experimental spectra and computed transition matrix elements has to be corrected for. The XRS spectra of light elements computed using FEFF are typically shifted by the order of 1 eV with respect to the experimental energy scale.<sup>43</sup> In this work, the theoretical energy scale was shifted by 0.8 eV so that the edges of the computed and experimental XRS spectra were coincident. However, due to the slightly different shape of these spectra at the edge region, the size of the energy shift is somewhat arbitrary. Fortunately, as the magnitude of the transition matrix elements change slowly as a function of energy, the exact size of the shift has only a small effect on the results. The obtained  $\ell$ -DOSs computed using additional

energy shifts of  $\pm 1$  eV differed only by having a slightly different slope in the near edge region.

As a result, we conclude that these factors do not hinder the interpretation of the data in terms of the  $\ell$ -DOS. The uncertainty in the  $\ell$ -DOS can be estimated analytically from the finite statistical accuracy of the experimental data. The fine structure of the  $\ell$ -DOS is apparently stable with respect to the abovementioned factors. The absolute intensity of the  $s$ - and  $p$ -DOS is, however, somewhat affected. In some cases, even the slope of the results may slightly change. Nevertheless, it should be noted that the relative intensities of the  $\ell$ -DOS components are much more stable than absolute ones.

## V. CONCLUSIONS

We have used the momentum transfer dependence of XRS together with a computational scheme to find the experimental  $\ell$ -DOS of diamond. We have observed the  $1s$  core exciton, shown that within the experimental resolution, its angular symmetry is dominantly  $p$ -like, and found no evidence of an  $s$ -type excitonic state. Moreover, we have systematically analyzed possible error sources of the current scheme in detail. Our results demonstrate that the shape of the experimental  $\ell$ -DOS is stable. However, the overall intensity of the  $\ell$ -DOS on the absolute scale is subject to slight variations.

## ACKNOWLEDGMENTS

This work was supported by the Academy of Finland (Contract no. 201291/205967/1110571) and the Research Funds of the University of Helsinki. The authors would like to thank Pieter Glatzel for lending us the Ge analyzer crystal.

- 
- <sup>1</sup>K.-W. Lee and W. E. Pickett, Phys. Rev. Lett. **93**, 237003 (2004).  
<sup>2</sup>P. Tamarat *et al.*, Phys. Rev. Lett. **97**, 083002 (2006).  
<sup>3</sup>C. Santori *et al.*, Phys. Rev. Lett. **97**, 247401 (2006).  
<sup>4</sup>L. Childress, J. M. Taylor, A. S. Sørensen, and M. D. Lukin, Phys. Rev. Lett. **96**, 070504 (2006).  
<sup>5</sup>G. S. Painter, D. E. Ellis, and A. R. Lubinsky, Phys. Rev. B **4**, 3610 (1971).  
<sup>6</sup>W. Hanke and L. J. Sham, Phys. Rev. Lett. **33**, 582 (1974).  
<sup>7</sup>M. S. Hybertsen and S. G. Louie, Phys. Rev. Lett. **55**, 1418 (1985).  
<sup>8</sup>L. X. Benedict, E. L. Shirley, and R. B. Bohn, Phys. Rev. B **57**, R9385 (1998).  
<sup>9</sup>W. A. Caliebe, J. A. Soininen, E. L. Shirley, C.-C. Kao, and K. Hämäläinen, Phys. Rev. Lett. **84**, 3907 (2000).  
<sup>10</sup>J. A. Soininen and E. L. Shirley, Phys. Rev. B **64**, 165112 (2001).  
<sup>11</sup>J. A. Soininen, K. Hämäläinen, W. A. Caliebe, C.-C. Kao, and E. L. Shirley, J. Phys.: Condens. Matter **13**, 8039 (2001).  
<sup>12</sup>M. Taillefumier, D. Cabaret, A.-M. Flank, and F. Mauri, Phys. Rev. B **66**, 195107 (2002).  
<sup>13</sup>J. F. Morar, F. J. Himpsel, G. Hollinger, G. Hughes, and J. L. Jordan, Phys. Rev. Lett. **54**, 1960 (1985).  
<sup>14</sup>H. W. L. Alves, H. Chacham, J. L. A. Alves, and J. R. Leite, Solid State Commun. **67**, 495 (1988).  
<sup>15</sup>K. A. Jackson and M. R. Pederson, Phys. Rev. Lett. **67**, 2521 (1991).  
<sup>16</sup>J. Nithianandam, Phys. Rev. Lett. **69**, 3108 (1992).  
<sup>17</sup>P. E. Batson, Phys. Rev. Lett. **70**, 1822 (1993).  
<sup>18</sup>W. Schülke, *Inelastic Scattering by Electronic Excitations, Handbook of Synchrotron Radiation* Vol. 3 (Elsevier, Amsterdam, 1991), pp. 565–637.  
<sup>19</sup>A. Mattila, J. A. Soininen, S. Galambosi, S. Huotari, G. Vanko, N. D. Zhigadlo, J. Karpinski, and K. Hamalainen, Phys. Rev. Lett. **94**, 247003 (2005).  
<sup>20</sup>S. Galambosi, M. Knaapila, J. Soininen, K. Nygard, S. Huotari, F. Galbrecht, U. Scherf, A. Monkman, and K. Hamalainen, *Macromolecules* **39**, 9261 (2006).  
<sup>21</sup>P. Wernet *et al.*, Science **304**, 995 (2004).  
<sup>22</sup>K. Hämäläinen, S. Galambosi, J. A. Soininen, E. L. Shirley, J.-P. Rueff, and A. Shukla, Phys. Rev. B **65**, 155111 (2002).  
<sup>23</sup>C. Sternemann, M. Volmer, J. A. Soininen, H. Nagasawa, M. Paulus, H. Enkisch, G. Schmidt, M. Tolan, and W. Schülke, Phys. Rev. B **68**, 035111 (2003).  
<sup>24</sup>C. Sternemann, J. A. Soininen, S. Huotari, G. Vanko, M. Volmer, R. A. Secco, J. S. Tse, and M. Tolan, Phys. Rev. B **72**, 035104 (2005).  
<sup>25</sup>J. A. Soininen, A. L. Ankudinov, and J. J. Rehr, Phys. Rev. B **72**,

- 045136 (2005).
- <sup>26</sup>J. A. Soininen, A. Mattila, J. J. Rehr, S. Galambosi, and K. Hämäläinen, *J. Phys.: Condens. Matter* **18**, 7327 (2006).
- <sup>27</sup>A. Mattila, J. A. Soininen, S. Galambosi, T. Pylkkänen, S. Huotari, N. D. Zhigadlo, J. Karpinski, and K. Hämäläinen (unpublished).
- <sup>28</sup>Y. Mizuno and Y. Ohmura, *J. Phys. Soc. Jpn.* **22**, 445 (1967).
- <sup>29</sup>K. Tohji and Y. Udagawa, *Phys. Rev. B* **39**, 7590 (1989).
- <sup>30</sup>H. Nagasawa, S. Mourikis, and W. Schülke, *J. Phys. Soc. Jpn.* **58**, 710 (1989).
- <sup>31</sup>A. L. Ankudinov, B. Ravel, J. J. Rehr, and S. D. Conradson, *Phys. Rev. B* **58**, 7565 (1998).
- <sup>32</sup>A. L. Ankudinov, C. E. Bouldin, J. J. Rehr, J. Sims, and H. Hung, *Phys. Rev. B* **65**, 104107 (2002).
- <sup>33</sup>K. Hermann *et al.*, STOBE-DEMON, version 1.0., StoBe Software, 2002.
- <sup>34</sup>Y. Ma, N. Wassdahl, P. Skytt, J. Guo, J. Nordgren, P. D. Johnson, J.-E. Rubensson, T. Boske, W. Eberhardt, and S. D. Kevan, *Phys. Rev. Lett.* **69**, 2598 (1992).
- <sup>35</sup>L. Fayette, B. Marcus, M. Mermoux, G. Tourillon, K. Laffon, P. Parent, and F. Le Normand, *Phys. Rev. B* **57**, 14123 (1998).
- <sup>36</sup>A. Gloter, A. Douiri, M. Tence, and C. Colliex, *Ultramicroscopy* **96**, 385 (2003).
- <sup>37</sup>W. Schülke, U. Bonse, H. Nagasawa, A. Kaprolat, and A. Berthold, *Phys. Rev. B* **38**, 2112 (1988).
- <sup>38</sup>R. D. Leapman, P. Rez, and D. F. Mayers, *J. Chem. Phys.* **72**, 1232 (1980).
- <sup>39</sup>P. E. Batson, *Phys. Rev. B* **47**, 6898 (1993).
- <sup>40</sup>F. Mauri and R. Car, *Phys. Rev. Lett.* **75**, 3166 (1995).
- <sup>41</sup>P. R. Bevington, *Data Reduction and Error Analysis for the Physical Sciences* (McGraw-Hill, New York, 1969).
- <sup>42</sup>C. L. Lawson and R. J. Hanson, *Solving Least Squares Problems* (Prentice-Hall, New Jersey, 1974).
- <sup>43</sup>A. L. Ankudinov, S. D. Conradson, J. Mustre de Leon, and J. J. Rehr, *Phys. Rev. B* **57**, 7518 (1998).